Biodegradable and drug-eluting inorganic composites based on mesoporous zinc oxide for urinary stent applications

Stability of a non-local kinetic model for cell migration with density dependent speed

Nadia Loy * Luigi Preziosi*†

September 7, 2020

Abstract

The aim of this article is to study the stability of a non-local kinetic model proposed in [17] in which the cell speed is affected by the cell population density non-locally measured and weighted according to a sensing kernel in the direction of polarization and motion. We perform the analysis in in a d-dimensional setting and we study the dispersion relation in the one-dimensional case and we show that the stability depends on two dimensionless parameters, the first one representing the stiffness of the system related to the cell turning rate, to the mean speed at equilibrium, and to the sensing radius, while the second one relates to the derivative of the mean speed with respect to the density evaluated at the equilibrium. It is proved that for Dirac delta sensing kernels centered at a finite distance, corresponding to sensing limited to a given distance from the cell center, the homogeneous configuration is linearly unstable to short waves. On the other hand, for a uniform sensing kernel, corresponding to uniformly weighting the information collected up to a given distance, the most unstable wavelength is identified and consistently matches with the numerical solution of the kinetic equation.

Keywords: Kinetic model, Non-local sensing, Stability, Cell migration, Volume filling

1 Introduction

Cell migration is greatly affected by the external environment: chemical and mechanical cues influence both cell polarization and speed. In particular, there are factors, such as nutrient and growth factors, that act as attractants or repellents, affecting the choice of polarization of the cell that determines the direction of cell migration. On the other hand, external cues with mechanical origin, such as density or stiffness of the extracellular matrix, may influence its speed. In order to polarize and move, cells sense their outer environment by extending their protrusions over a distance that can reach several cell diameters, and translate the sampled information into the choice of a direction and speed. In collective migration processes, one of the most important cues that is sensed is the presence of other cells in the neighborhood and, in an averaged sense, the macroscopic density of the cell population. For example, cell-cell adhesion is the mechanism that is at the basis of collective cell-migration, leading to reciprocal attraction and formation of cell clusters. On the other hand, overcrowding may slow down or hamper a cell from passing through regions with too many cells.

In order to describe such non-local sampling of the environment, several mathematical models have been recently proposed in the literature. Regarding macroscopic models, in [20] and then in [13] the authors introduced a finite sampling radius and defined a non-local gradient affecting cell velocity as the average of an external field over a surface representing the membrane of the cell. The authors of [1] proposed a macroscopic integro-differential equation modelling cell-cell

*Department of Mathematical Sciences "G. L. Lagrange", Politecnico di Torino, Corso Duca degli Abruzzi 24, 10129 Torino, Italy (nadia.loy@polito.it)

†Corresponding author: (luigi.preziosi@polito.it)

adhesion, where the integral over a finite radius is in charge of describing a non-local sensing of the cell density. The model is then extended in [15] to deal with haptotaxis and chemotaxis, also focusing on well-posedness issues.

Such models are in general postulated at the macroscopic level, but many efforts have been made in order to derive them from a microscopic or mesoscopic description. The microscopic dynamics of swimming bacteria may be usually described as a 'run and tumble' process, that is the alternation of 'runs' over straight lines and re-orientations. Run and tumble is classically described by a stochastic process called velocity jump process [24], whose key features are the frequency of re-orientations and the transition probability that describes the choice of a new orientation and speed after the 'tumble'. This microscopic mechanism may be implemented in a transport kinetic equation [19, 24] in order to obtain a mesoscopic description. Also eukariotic cells, when migrating individually, change their polarization and direction of migration as they sense a varying environment along their path and perform a (biased) random motion that may be described by a velocity jump process [12].

In [9] the authors proposed a non-local kinetic model in which all cells have the same fixed speed but can change their orientation because of repulsion, alignment and attraction. Its numerical integration showed a wide variety of patterns. The linear stability analysis of the model is then performed in [8]. In particular, the authors showed a zig-zag behaviour that is due to the change of the direction caused by the fact that the population had reached point wise a threshold density.

In [16] we proposed a non-local kinetic model with double-bias, *i.e.*, taking into account the presence of a double environmental cue. The first cue affects the choice of the direction and the second one, usually of mechanical origin, affects the speed that the cell can achieve going in that direction. Therefore, the turning operator is composed of two integrals, the first one determining the probability of polarizing in a certain direction after averaging the sensing of a chemical or mechanical cue over a finite neighborhood, and the second one setting the probability of moving with a certain speed in the chosen direction after averaging the sensing of another chemical or mechanical cue over a possibly different finite neighborhood. The process of measuring the external environment may be localized on the membrane, or the cell may average the cues over a surface or a volume. This corresponds in the model to different sensing kernels, that may be a Dirac delta, if the sampling is localized at a fixed distance from the cell center, or a Heaviside function, if the sampling is uniformly averaged over the sensing distance, or a decreasing function if the cell samples with its protrusions the closer environment more often and in more detail than farther points and averages the amount of information measured.

The model was then extended in [17] to take into account physical limits of migration. In fact, physically constraining situations, such as too dense extracellular matrix or cell overcrowding, might hamper the real possibility of cells of measuring beyond physical barriers or to move in certain regions. In particular, we included the fact that the decision on the speed is based on the information sensed in an area in which the cell is actually able to move and collect information by extending its protrusions. Therefore, the sensing radius will be different in every position and time and in every direction according, for instance, to the sensed macroscopic density.

In [16] and [17] it was numerically shown that the presence of density dependent cues, may generate instabilities and the formation of patterns, which may vary depending on the sensing kernel and on several modelling parameters. In particular, volume filling [17] was shown to reproduce a zig-zag behaviour similar to the one reported in [8]. The linear stability of a kinetic model describing cell migration affected by a density dependent bias on the choice of the direction of movement was studied in [18]. It was shown that the formation of patterns is ruled by a non-dimensional parameter that measures both the stiffness of the system and the stiffness of the response to the measured surrounding density.

Similar patterns occur in other systems that present a density dependent velocity. A typical example is traffic flow. It is common experience, obviously confirmed experimentally [14], that the speed and traffic flux depend on the traffic density itself giving rise to stop-and-go patterns for high densities. So-called *fundamental diagrams of traffic flow, that relate the flow to the traffic density,* show that there exists a threshold value of the density above which the traffic is *congested* while speed-dependent diagrams show that the mean speed depends on the traffic density. For

these kinds of flows, kinetic models in which the mean speed is a function of the local macro density of the traffic have been recently proposed in [11, 22, 23]. In particular, in [11, 23] the kinetic models implement velocity jump processes in which the transition probability depends on the macroscopic density of the traffic. Non-local models for traffic flow have been recently widely studied (see [6] for a review). In particular, the authors of [2] propose a macroscopic hyperbolic model with non-local flux in which the speed depends on a weighted mean of the downstream traffic density as drivers adapt their velocity with respect to what happens in front of them. In these models the flux function depends on a convolution term between the density of vehicles and a kernel function defined on the positive real domain.

The aim of the present work is to study the stability of the homogeneous equilibrium configurations of the model proposed in [17] when there is an isotropic polarization and a density dependent cue influencing the cell speed. We adopt the same approach used in [18], but the methodology to study the stability properties is different because of the differences in the transition term.

After briefly recalling the model in Section 2, Section 3 is devoted to the study of the linear stability of a homogeneous equilibrium configuration with macroscopic density smaller than the threshold one representing cell congestion and, therefore, a physical limit of migration. Specifically, after determining an integral relationship between the growth rate of the perturbation and its wavelength in the general d-dimensional case, in Section 3.1 we focus on the one-dimensional case with a Dirac delta distribution function for the speed because it allows to obtain some analytical results. In fact, in Section 3.2 an analysis with respect to short waves shows the instability of the homogeneous equilibrium configuration if the sensing strategy is localized (*i.e.*, the sensing kernel is a Dirac delta measuring what happens at a given distance from the cell center) for any value of the parameters. On the other hand, for kernels presenting a discontinuity at the maximum sensing radius (*e.g.*, a Heaviside function leading to uniform sensing) instability to short waves is present only for sufficiently high values of the two dimensionless parameters. Finally, if the sensing kernel is smooth and vanishes above a maximum sensing radius, then the homogeneous equilibrium configuration is always stable to short waves. The analysis with respect to long waves leads to a stability condition as well. The dispersion relation is described numerically for all wave numbers in Section 3.3. For a Dirac delta sensing kernel short waves are the most unstable, while for more regular kernels they are not, with the maximum growth rate achieved for finite wave numbers. Then, Section 4 is devoted to the discussion of the results obtained by a numerical integration of the kinetic model with a von Mises distribution for cell speed, with the aim of checking how and to which extent the developed patterns are consistent with the linear stability analysis. It is found that for a uniform kernel and a decreasing kernel the patterns are triggered at wavelengths comparable with the theoretical linear stability study. We also show that for a Dirac delta sensing kernel patterns are developed at shorter wavelengths. Finally, Section 5 draws some conclusions.

2 The mathematical model

We shall consider a statistical description of the cell population through the distribution density $p = p(t, \mathbf{x}, v, \hat{\mathbf{v}})$ parametrized by time $t > 0$, position $\mathbf{x} \in \Omega \subseteq \mathbb{R}^d$, speed $v \in [0, U]$, where U is the maximum speed a cell can achieve, and polarization direction $\hat{\mathbf{v}} \in \mathbb{S}^{d-1}$, where $\mathbb{S}^{d-1} = \{\hat{\mathbf{v}} \in \mathbb{R}^d : \ |\hat{\mathbf{v}}| = 1\}$. The density distribution p depends separately on the direction $\hat{\mathbf{v}}$ and on the speed v because of the need of separating polarization and motility mechanisms. In particular, in the following we shall consider a situation in which cell polarization is random. On the other hand, cells have a direction-dependent motility in response of the density of the cell population itself. In fact, cells may be too packed, thus hampering cell motility, or may be less dense, thus favouring it. The macroscopic density of the statistical distribution of particles may be recovered as

$$\rho(t, \mathbf{x}) = \int_{\mathbb{S}^{d-1}} \int_0^U p(t, \mathbf{x}, v, \hat{\mathbf{v}}) \, dv \, d\hat{\mathbf{v}}. \tag{1}$$

The mesoscopic model consists of the transport equation for the cell distribution

$$\frac{\partial p}{\partial t}(t,\mathbf{x},v,\hat{\mathbf{v}}) + v\hat{\mathbf{v}}\cdot\nabla p(t,\mathbf{x},v,\hat{\mathbf{v}}) = \mathcal{J}[p](t,\mathbf{x},v,\hat{\mathbf{v}})\,, \tag{2}$$

where the operator ∇ denotes the spatial gradient and the term $v\hat{\mathbf{v}}\cdot\nabla p(t,\mathbf{x},v,\hat{\mathbf{v}})$ takes into account the free transport. The change of the microscopic velocity is modelled by the term $\mathcal{J}[p](\cdot,v,\hat{\mathbf{v}})$, named *turning operator*, which is an integral operator, where the dot stands for the time and space variables. It characterizes a velocity jump process as introduced by [24] and then by [19]. Its general form is

$$\begin{aligned}\mathcal{J}[p](\cdot,v,\hat{\mathbf{v}}) = \mu(\mathbf{x})\int_{\mathbb{S}^{d-1}}\int_0^U T[\rho](\cdot,v,\hat{\mathbf{v}}|'v,'\hat{\mathbf{v}})p(\cdot,'v,'\hat{\mathbf{v}})\,d'v\,d'\hat{\mathbf{v}}\\ - \mu(\mathbf{x})\int_{\mathbb{S}^{d-1}}\int_0^U T[\rho](\cdot,v',\hat{\mathbf{v}}'|v,\hat{\mathbf{v}})p(\cdot,v,\hat{\mathbf{v}})\,dv'd\hat{\mathbf{v}}',\end{aligned} \tag{3}$$

where $'\mathbf{v} = {}'v'\hat{\mathbf{v}}$ is the pre-turning velocity of the gain term and $\mathbf{v}' = v'\hat{\mathbf{v}}'$ is the post-turning velocity of the loss term. The so-called *turning kernel* $T[\rho](\cdot,v,\hat{\mathbf{v}}|'v,'\hat{\mathbf{v}})$ is the probability density distribution for a cell in $\mathbf{x}$ at time t of re-orienting along $\hat{\mathbf{v}}$ and moving with speed v given the pre-turning polarization direction $'\hat{\mathbf{v}}$ and speed $'v$. Then, T is a conditional *transition probability density* on $[0,U]\times\mathbb{S}^{d-1}$ that is influenced by a measuring of the cell density ρ sensed by the cell. We adopted here the notation $T = T[\rho](\cdot,v,\hat{\mathbf{v}})$ because the dependence of T on t and $\mathbf{x}$ is through a sampling of ρ. The quantity $\mu(\mathbf{x})$ is the turning frequency of cells located in $\mathbf{x}$.

Being a transition probability density, $T[\rho]$ satisfies

$$\int_{\mathbb{S}^{d-1}}\int_0^U T[\rho](\cdot,v,\hat{\mathbf{v}}|'v,'\hat{\mathbf{v}})\,dv\,d\hat{\mathbf{v}} = 1\,,\qquad \forall\mathbf{x}\in\Omega,\ \forall('v,'\hat{\mathbf{v}})\in[0,U]\times\mathbb{S}^{d-1}, \tag{4}$$

which allows to simplify (3) to

$$\mathcal{J}[p](\cdot,v,\hat{\mathbf{v}}) = \mu(\mathbf{x})\int_{\mathbb{S}^{d-1}}\int_0^U T[\rho](\cdot,v,\hat{\mathbf{v}}|'v,'\hat{\mathbf{v}})p(t,\mathbf{x},'v,'\hat{\mathbf{v}})\,d'v\,d'\hat{\mathbf{v}} - \mu(\mathbf{x})p(t,\mathbf{x},v,\hat{\mathbf{v}})\,. \tag{5}$$

In [16, 17] the authors assumed that cells retain no memory of their velocity prior to their re-orientation, *i.e.*, $T[\rho] = T[\rho](\cdot,v,\hat{\mathbf{v}})$. This assumption has been used in the pioneering literature of this kind of models applied to cell migration [4, 5, 12, 24]. It is biologically justified by the fact that the process related to cell ruffling and sensing which is responsible for the biased re-orientation is very slow, but however excludes phenomena in which cell persistence is important. This assumption allows to simplify the *turning operator* in (5) to

$$\mathcal{J}[p](t,\mathbf{x},v,\hat{\mathbf{v}}) = \mu\Big[\rho(t,\mathbf{x})T[\rho](t,\mathbf{x},v,\hat{\mathbf{v}}) - p(t,\mathbf{x},v,\hat{\mathbf{v}})\Big]\,. \tag{6}$$

In [16] we introduced a model that takes into account the fact that during their motion cells are capable of detecting and measuring external signals through membrane receptors located along the cell's protrusions that can extend over a finite radius. In particular, the transition probability takes into account a double environmental cue that influences the choice of the direction and of the speed on every possible direction. In [18] we analyzed the stability of a model that takes into account only the non-local sensing that influences to the choice of the direction. In that case, if the quantity influencing cell orientation is the cell density ρ, the transition probability writes

$$T[\rho](t,\mathbf{x},v,\hat{\mathbf{v}}) = c(t,\mathbf{x})\int_0^{+\infty}\gamma(\lambda)f(\rho(t,\mathbf{x}+\lambda\hat{\mathbf{v}}))\,d\lambda\,\psi(v)\,,$$

where f determines how the density in the different directions is measured in order to choose the most probable polarization. On the other hand, the choice of the speed is independent of the

polarization direction and is not biased by external factors.

In the present work, the situation is somewhat specular: polarization is random, *i.e.* cells do not perform a non-local sampling of a substance to set a preferred direction of motion, but their speed is influenced in every possible direction by a non-local sensing of an environmental cue of mechanical origin. In particular, we shall consider density-dependent effects.

Following [16, 17], the transition probability then reads

$$T[\rho](t,\mathbf{x},v,\hat{\mathbf{v}}) = c(t,\mathbf{x}) \int_0^{R_\rho(t,\mathbf{x},\hat{\mathbf{v}})} \gamma(\lambda)\psi(v|\rho(t,\mathbf{x}+\lambda\hat{\mathbf{v}}))\, d\lambda, \tag{7}$$

where $c(t,\mathbf{x})$ is a normalization factor, so that the integral of T over the velocity space is one and (4) is satisfied. In this way, T is a mass preserving transition probability. The function

$$\psi = \psi(v|\rho) : [0,U] \longmapsto \mathbb{R}_+ \tag{8}$$

is the probability density distribution of the speeds that is conditioned by the cell density. In particular, $\psi(v|\rho(\mathbf{x}+\lambda\hat{\mathbf{v}}))\, dv$ is the probability that the speed of a cell located in $\mathbf{x}$ and oriented along $\hat{\mathbf{v}}$ is in $[v, v+dv]$. The resulting speed is influenced by the value of ρ measured in $\mathbf{x}+\lambda\hat{\mathbf{v}}$ mediated over the sensing radius R_ρ weighted by a function γ, that with an abuse on designation is convenient to call here sensing kernel. The function ψ is therefore in $L^1([0,U])$ and it normalizes to one being a probability density distribution, *i.e.*,

$$\int_0^U \psi(v|\rho)\, dv = 1, \quad \forall \rho \geq 0. \tag{9}$$

The sensing kernel γ is assumed to have a compact support in $[0,R]$ where R is the maximum length of a protrusion from the cell center, that is related to the finite size of the influencing neighborhood. It may be a Dirac delta, i.e., $\gamma(\lambda) = \delta(\lambda - R)$, if cells only use the information perceived on a surface of given radius R, a Heaviside function, i.e., $\gamma(\lambda) = H(\lambda - R)$ if cells explore the whole volume of the sphere centered in $\mathbf{x}$ with radius R and uniformly weight the information sensed, or it may be a decreasing function of the distance λ from the cell center $\mathbf{x}$ taking for instance into account that the probability of making longer protrusions decreases with the distance, so the sensing of closer regions is more accurate.

If γ is regular enough, as we can invert the order of integration and (9) holds, we have that the normalization factor simplifies to

$$c(t,\mathbf{x}) = \frac{1}{\displaystyle\int_{\mathbb{S}^{d-1}} \int_0^U \int_0^{R_\rho(t,\mathbf{x},\hat{\mathbf{v}})} \gamma(\lambda)\psi(v|\rho(t,\mathbf{x}+\lambda\hat{\mathbf{v}}))\, d\lambda dv\, d\hat{\mathbf{v}}} = \frac{1}{\displaystyle\int_{\mathbb{S}^{d-1}} \Gamma_\rho(t,\mathbf{x},\hat{\mathbf{v}}) d\hat{\mathbf{v}}}$$

where

$$\Gamma_\rho(t,\mathbf{x},\hat{\mathbf{v}}) = \int_0^{R_\rho(t,\mathbf{x},\hat{\mathbf{v}})} \gamma(\lambda)\, d\lambda.$$

The upper limit of integration R_ρ is introduced to take into account the presence of physical limits of migration caused by the macroscopic cell density, *i.e.*, the presence of regions that are so overcrowded (say, with density above a threshold value ρ_{th}) to hamper cells from moving and extending their protrusions. Therefore, their length and therefore R_ρ will depend on the position and direction of extension. Specifically, R_ρ is the minimum between R and the maximum distance that a protrusion can reach and that the cell uses to set its speed in the possible presence of obstacles and physical limits of migration in a certain direction of motion. Referring to [17] for a detailed discussion, it is defined as

$$R_\rho(t,\mathbf{x},\hat{\mathbf{v}}) = \begin{cases} R \qquad \text{if} \quad \rho(t,\mathbf{x}+\lambda\hat{\mathbf{v}}) \leq \rho_{th}, \quad \forall \lambda \in [0,R)\,, \\ \\ \inf\{\lambda \in [0,R) : \rho(t,\mathbf{x}+\lambda\hat{\mathbf{v}}) > \rho_{th}\}, \quad \text{otherwise}, \end{cases} \tag{10}$$

where ρ_{th} is a threshold value of the cell density characterizing the physical limit of migration, *i.e.* the threshold value that the cell density can not overcome.

The transport equation (2) therefore reads

$$\frac{\partial p}{\partial t}(t,\mathbf{x},v,\hat{\mathbf{v}}) + v\hat{\mathbf{v}}\cdot\nabla p(t,\mathbf{x},v,\hat{\mathbf{v}}) =$$

$$\mu\left[\frac{\rho(t,\mathbf{x})}{\displaystyle\int_{\mathbb{S}^{d-1}}\Gamma_\rho(t,\mathbf{x},\hat{\mathbf{v}})d\hat{\mathbf{v}}}\int_0^{R_\rho(t,\mathbf{x},\hat{\mathbf{v}})}\gamma(\lambda)\psi(v|\rho(t,\mathbf{x}+\lambda\hat{\mathbf{v}}))\,d\lambda - p(t,\mathbf{x},v,\hat{\mathbf{v}})\right]. \tag{11}$$

The first and most important point in specifying the choice of $\psi(v|\rho)$ consists in identifying how the average speed

$$\bar{v}(\rho) = \int_0^U v\psi(v|\rho)\,dv\,, \tag{12}$$

depends on the macroscopic density. In particular, as cells are slowed down by the presence of high cell densities, we shall choose an average speed that is a decreasing function of the cell population density. An example of average speed taking into account volume filling effects is

$$\bar{v}(\rho) = \bar{v}_M\left(1-\frac{\rho}{\rho_{th}}\right)_+, \tag{13}$$

where $(\cdot)_+ = \max(\cdot,0)$ is the positive part operator. This choice prescribes the full arrest of a cell that measures densities above a critical value ρ_{th}, while the mean speed is maximum and equal to $\bar{v}_M$ in the limit of a very small macroscopic density.

Then, an example of probability distribution density is the beta distribution

$$\psi(v|\rho) = \frac{3v(2\bar{v}(\rho)-v)_+}{4\bar{v}^3(\rho)}\,, \tag{14}$$

if $\bar{v}(\rho) > 0$ getting to a Dirac delta in the limit of vanishing $\bar{v}(\rho)$, which occurs when $\rho \geq \rho_{th}$. If we choose (14) then the maximum allowed microscopic speed is $U = 2\bar{v}_M$. In the following the probability density distribution that will be mostly used is the Dirac delta function $\psi(v|\rho) = \delta(v-\bar{v}(\rho))$, because it allows to perform analytical computations. In this case $U = \bar{v}_M$.

As discussed in [17] and using standard arguments [3] we observe that the local asymptotic equilibrium states (provided perfect reflection boundary conditions) are given by

$$p(t,\mathbf{x},v,\hat{\mathbf{v}}) = \rho(t,\mathbf{x})T[\rho](t,\mathbf{x},v,\hat{\mathbf{v}}). \tag{15}$$

The equilibrium configuration will be uniform only if the density ρ_∞ corresponding to p_∞ (and $T[\rho_\infty]$ as a consequence) is constant.

The aim of this paper is then to study the linear stability of the homogeneous equilibrium configurations given by

$$p_\infty(v,\hat{\mathbf{v}}) = \rho_\infty T[\rho_\infty](v,\hat{\mathbf{v}}). \tag{16}$$

In particular, the case of interest is the one in which $\rho_\infty < \rho_{th}$ and therefore we will consider initial conditions $\rho_0(\mathbf{x})$ that are small perturbations of the uniform solution ρ_∞, such that

$$\rho_0(\mathbf{x}) < \rho_{th} \quad \forall\mathbf{x}\in\Omega \qquad \text{and} \qquad \int_\Omega \rho(0,\mathbf{x})d\mathbf{x} = \rho_\infty|\Omega|\,,$$

as the mass in conserved.

In fact, if on the contrary $\rho_0(\mathbf{x})$ is a small perturbation of $\rho_\infty > \rho_{th}$, then the system is frozen, because cells are in a congested condition. In fact, the average speed $\bar{v}(\rho_0(\mathbf{x}))$ in (13) vanishes.

Therefore, in the conditions of our interest $R_\rho(t,\mathbf{x},\hat{\mathbf{v}}) = R$ is homogeneous in space and does not depend on the orientation. In addition, in the range of application of the linear stability analysis, (13) never vanishes, which implies that the presence of the positive part is unessential.

3 Linear stability analysis

We want to study the stability of the homogeneous configurations (16) corresponding to a constant density $\rho_\infty < \rho_{th}$. Denoting by $\bar{v}(\rho_\infty)$ the average speed (12) achieved at ρ_∞ we can introduce the following dimensionless variables

$$\tilde{\mathbf{x}} = \frac{\mathbf{x}}{R}, \quad \tilde{v} = \frac{v}{\bar{v}(\rho_\infty)}, \quad \tilde{t} = \frac{\bar{v}(\rho_\infty)t}{R}, \quad \tilde{\rho} = \frac{\rho}{\rho_\infty}, \quad \tilde{p} = \frac{\bar{v}(\rho_\infty)p}{\rho_\infty}, \quad \tilde{\psi} = \bar{v}(\rho_\infty)\psi\,, \tag{17}$$

and work with the dimensionless form of (11) that has a similar structure, with $R_\rho = R$ replaced by 1 and $1/\mu$ by the dimensionless number

$$\mathcal{V} = \frac{\bar{v}(\rho_\infty)}{R\mu}\,. \tag{18}$$

Coherently, we will also denote by $\tilde{U} = U/\bar{v}(\rho_\infty)$ and $V(\tilde{\rho}) = \bar{v}(\rho)/\bar{v}(\rho_\infty)$. According to this dimensionless notation the homogeneous steady state will trivially be $\tilde{\rho}_\infty = 1$ and, obviously, $V(\tilde{\rho}_\infty = 1) = 1$. As we shall see, another dimensionless number that will be relevant in the linear stability analysis is

$$M = -V'(1). \tag{19}$$

The negative sign is due to the fact that it is convenient to work with a positive parameter M and the mean speed decreases when the density increases. The dimensionless form of (13) is

$$V(\tilde{\rho}) = \frac{\bar{v}(\rho)}{\bar{v}(\rho_\infty)} = \frac{1 - \dfrac{\tilde{\rho}}{\tilde{\rho}_{th}}}{1 - \dfrac{1}{\tilde{\rho}_{th}}}\,,$$

and

$$M = \frac{1}{\tilde{\rho}_{th} - 1} = \frac{\rho_\infty}{\rho_{th} - \rho_\infty}, \tag{20}$$

that is positive as $\rho_\infty < \rho_{th}$.

For the sake of simplicity in rewriting the transport equation

$$\frac{\partial p}{\partial t}(t, \mathbf{x}, v, \hat{\mathbf{v}}) + v\hat{\mathbf{v}}\cdot\nabla p(t, \mathbf{x}, v, \hat{\mathbf{v}}) = \frac{1}{\mathcal{V}}\left[\frac{\rho(t, \mathbf{x})}{\Gamma|\mathbb{S}^{d-1}|}\int_{\mathbb{R}_+}\gamma(\lambda)\psi(v|\rho(t, \mathbf{x} + \lambda\hat{\mathbf{v}}))\,d\lambda - p(t, \mathbf{x}, v, \hat{\mathbf{v}})\right], \tag{21}$$

we drop the tildes and extend the integral over $\mathbb{R}_+$, upon considering that γ has compact support in $[0, 1]$. In addition,

$$\Gamma = \int_{\mathbb{R}_+}\gamma(\lambda)d\lambda = \int_0^1 \gamma(\lambda)d\lambda\,,$$

and $|\mathbb{S}^{d-1}|$ is the surface of $\mathbb{S}^{d-1}$.

The nondimensionalized local asymptotic equilibrium state of (21) is (see (16))

$$p_\infty = \frac{1}{|\mathbb{S}^{d-1}|}\psi(v|1)\,, \tag{22}$$

where the value 1 in ψ corresponds to the dimensionless reference density that will be perturbed for the stability analysis. We then consider a small perturbation of the homogeneous solution above $p(t, \mathbf{x}, v, \hat{\mathbf{v}}) = p_\infty(v) + \hat{p}(t, \mathbf{x}, v, \hat{\mathbf{v}})$ and observe that $\rho(t, \mathbf{x}) = 1 + \hat{\rho}(t, \mathbf{x})$ where

$$\hat{\rho}(t, \mathbf{x}) = \int_{\mathbb{R}_+\times\mathbb{S}^{d-1}}\hat{p}(t, \mathbf{x}, v, \hat{\mathbf{v}})dv\,d\hat{\mathbf{v}}\,.$$

The linearization of T then leads to

$$T[\hat{\rho}] = \frac{1}{\Gamma|\mathbb{S}^{d-1}|}\int_{\mathbb{R}_+}\gamma(\lambda)\psi(v|1+\hat{\rho}(t,\mathbf{x}+\lambda\hat{\mathbf{v}}))\,d\lambda \approx \frac{1}{|\mathbb{S}^{d-1}|}\psi(v|1)+\frac{1}{\Gamma|\mathbb{S}^{d-1}|}\int_{\mathbb{R}_+}\gamma(\lambda)\hat{\rho}(t,\mathbf{x}+\lambda\hat{\mathbf{v}})\,d\lambda\,\frac{\partial\psi}{\partial\rho}(v|1)\,, \tag{23}$$

because

$$\psi(v|1+\hat{\rho}(t,\mathbf{x}+\lambda\hat{\mathbf{v}})) \approx \psi(v|1)) + \frac{\partial\psi}{\partial\rho}(v|1)\hat{\rho}(t,\mathbf{x}+\lambda\hat{\mathbf{v}}).$$

The term $\dfrac{\partial\psi}{\partial\rho}(v|1)$ denotes the partial derivative of ψ with respect to ρ, that is the conditional variable that enters in the definition of the density distribution ψ (see, for instance, (14) with (13)), obviously considering the other parameters fixed. We observe that the mass of $\dfrac{\partial\psi}{\partial\rho}(v|1)$ has the following property

$$\int_0^U \frac{\partial\psi}{\partial\rho}(v|1)\,dv = \frac{\partial}{\partial\rho}\int_0^U \psi(v|1)\,dv = 0,$$

which implies that the perturbed transition probability (23) is mass preserving.

The perturbed equation related to (21) to be used to study the linear stability then becomes

$$\begin{aligned}&\frac{\partial\hat{p}}{\partial t}(t,\mathbf{x},v,\hat{\mathbf{v}}) + v\hat{\mathbf{v}}\cdot\nabla\hat{p}(t,\mathbf{x},v,\hat{\mathbf{v}}) = \\ &\frac{1}{\mathcal{V}}\left[\frac{\hat{\rho}(t,\mathbf{x})}{|\mathbb{S}^{d-1}|}\psi(v|1) + \frac{1}{\Gamma|\mathbb{S}^{d-1}|}\int_{\mathbb{R}_+}\gamma(\lambda)\hat{\rho}(t,\mathbf{x}+\lambda\hat{\mathbf{v}})\,d\lambda\,\frac{\partial\psi}{\partial\rho}(v|1) - \hat{p}(t,\mathbf{x},v,\hat{\mathbf{v}})\right].\end{aligned} \tag{24}$$

Let us now consider perturbations of the form

$$\hat{p}(t,\mathbf{x},v,\hat{\mathbf{v}}) = g(v,\hat{\mathbf{v}})e^{i\mathbf{k}\cdot\mathbf{x}+\sigma t}, \tag{25}$$

where g has its density defined as

$$\rho_g = \int_{\mathbb{S}^{d-1}}\int_0^U g(v,\hat{\mathbf{v}})\,dv\,d\hat{\mathbf{v}}\,,$$

and, then, $\hat{\rho} = \rho_g e^{i\mathbf{k}\cdot\mathbf{x}+\sigma t}$. We observe that now $\mathbf{k}$ and σ are dimensionless and are linked to the corresponding dimensional wave number $\bar{\mathbf{k}}$ and growth rate $\bar{\sigma}$ by $\mathbf{k} = R\bar{\mathbf{k}}$ and $\sigma = \dfrac{R}{\bar{v}(\rho_\infty)}\bar{\sigma}$.

Substituting (25) in Eq. (24) gives

$$\begin{aligned}&\left(\sigma + i\mathbf{k}\cdot\hat{\mathbf{v}}v + \frac{1}{\mathcal{V}}\right)g(v,\hat{\mathbf{v}})e^{i\mathbf{k}\cdot\mathbf{x}+\sigma t} \\ &= \frac{1}{\mathcal{V}}\left[\frac{\psi(v|1)}{|\mathbb{S}^{d-1}|}\rho_g e^{i\mathbf{k}\cdot\mathbf{x}+\sigma t} + \frac{1}{\Gamma|\mathbb{S}^{d-1}|}\int_{\mathbb{R}_+}\gamma(\lambda)\rho_g e^{i\mathbf{k}\cdot(\mathbf{x}+\lambda\hat{\mathbf{v}})+\sigma t}\,d\lambda\,\frac{\partial\psi}{\partial\rho}(v|1)\right],\end{aligned} \tag{26}$$

and therefore

$$\left(\sigma + i\mathbf{k}\cdot\hat{\mathbf{v}}v + \frac{1}{\mathcal{V}}\right)g = \frac{1}{\mathcal{V}|\mathbb{S}^{d-1}|}\left[\psi(v|1) + \hat{\gamma}(\mathbf{k}\cdot\hat{\mathbf{v}})\frac{\partial\psi}{\partial\rho}(v|1)\right]\rho_g, \tag{27}$$

where we denoted by

$$\hat{\gamma}(\mathbf{k}\cdot\hat{\mathbf{v}}) = \frac{1}{\Gamma}\int_{\mathbb{R}_+}\gamma(\lambda)e^{i\mathbf{k}\cdot\hat{\mathbf{v}}\lambda}d\lambda\,,$$

a quantity clearly related to the Laplace transform of γ/Γ.

By writing g explicitly and then integrating over the velocity space we have that

$$1 = \frac{1}{\mathcal{V}|\mathbb{S}^{d-1}|}\int_{\mathbb{S}^{d-1}}\int_0^U \frac{\psi(v|1)+\dfrac{\partial\psi}{\partial\rho}(v|1)[\hat\gamma_c(\mathbf{k}\cdot\hat{\mathbf{v}})+i\hat\gamma_s(\mathbf{k}\cdot\hat{\mathbf{v}})]}{\sigma+\dfrac{1}{\mathcal{V}}+i\mathbf{k}\cdot\hat{\mathbf{v}}v}dv\,d\hat{\mathbf{v}}\,, \tag{28}$$

where

$$\hat\gamma_c(\mathbf{k}\cdot\hat{\mathbf{v}}) = \frac{1}{\Gamma}\int_{\mathbb{R}_+}\gamma(\lambda)\cos(\lambda\mathbf{k}\cdot\hat{\mathbf{v}})\,d\lambda\,, \quad \text{and} \quad \hat\gamma_s(\mathbf{k}\cdot\hat{\mathbf{v}}) = \frac{1}{\Gamma}\int_{\mathbb{R}_+}\gamma(\lambda)\sin(\lambda\mathbf{k}\cdot\hat{\mathbf{v}})\,d\lambda\,,$$

which is equivalent to the system

$$\int_{\mathbb{S}^{d-1}}\int_0^U \frac{\left[\psi(v|1)+\dfrac{\partial\psi}{\partial\rho}(v|1)\hat\gamma_c(\mathbf{k}\cdot\hat{\mathbf{v}})\right]\left(\sigma_r+\dfrac{1}{\mathcal{V}}\right)+\dfrac{\partial\psi}{\partial\rho}(v|1)\hat\gamma_s(\mathbf{k}\cdot\hat{\mathbf{v}})(\sigma_i+\mathbf{k}\cdot\hat{\mathbf{v}}v)}{\left(\sigma_r+\dfrac{1}{\mathcal{V}}\right)^2+(\sigma_i+\mathbf{k}\cdot\hat{\mathbf{v}}v)^2}dv\,d\hat{\mathbf{v}} = |\mathbb{S}^{d-1}|\mathcal{V}, \tag{29}$$

and

$$\int_{\mathbb{S}^{d-1}}\int_0^U \frac{\left[\psi(v|1)+\dfrac{\partial\psi}{\partial\rho}(v|1)\hat\gamma_c(\mathbf{k}\cdot\hat{\mathbf{v}})\right](\sigma_i+\mathbf{k}\cdot\hat{\mathbf{v}}v)-\dfrac{\partial\psi}{\partial\rho}(v|1)\hat\gamma_s(\mathbf{k}\cdot\hat{\mathbf{v}})\mathbf{k}\cdot\hat{\mathbf{v}}v\left(\sigma+\dfrac{1}{\mathcal{V}}\right)}{\left(\sigma_r+\dfrac{1}{\mathcal{V}}\right)^2+(\sigma_i+\mathbf{k}\cdot\hat{\mathbf{v}}v)^2}dv\,d\hat{\mathbf{v}} = 0, \tag{30}$$

where $\sigma = \sigma_r + i\sigma_i$.

A big simplification occurs in the one-dimensional case. In fact, in this case the integral over the sphere reduces to the sum of the evaluation of the integrand in the two points $\pm k$ and then (30) simplifies to

$$[\hat\gamma_s(k)+\hat\gamma_s(-k)]\left(\sigma_r+\frac{1}{\mathcal{V}}\right)-\left[\psi(v|1)+\frac{\partial\psi}{\partial\rho}(v|1)\hat\gamma_c(k)\right](\sigma_i+kv)-\left[\psi(v|1)+\frac{\partial\psi}{\partial\rho}(v|1)\hat\gamma_c(-k)\right](\sigma_i-kv) = 0\,.$$

Since $\hat\gamma_s$ and $\hat\gamma_c$ are an odd and an even function of k, respectively, the last equation reduces to

$$\left[\psi(v|1)+\frac{\partial\psi}{\partial\rho}(v|1)\hat\gamma_c(k)\right]\sigma_i = 0\,,$$

which is satisfied by $\sigma_i = 0$.

Therefore, σ is real and Eq. (29) reduces to

$$1 = \frac{1}{\mathcal{V}}\int_0^U \frac{\left(\psi(v|1)+\dfrac{\partial\psi}{\partial\rho}(v|1)\hat\gamma_c(k)\right)\left(\sigma+\dfrac{1}{\mathcal{V}}\right)+\dfrac{\partial\psi}{\partial\rho}(v|1)\hat\gamma_s(k)kv}{\left(\sigma+\dfrac{1}{\mathcal{V}}\right)^2+k^2v^2}\,dv. \tag{31}$$

3.1 Dirac delta speed distribution

The integral in (31) can be solved analytically only for few particular density distributions. For instance, in the case of the beta distribution (14), it leads to a transcendental relation with polynomial, logarithmic and $\tan^{-1}$ terms that can only be analyzed on the basis of numerical evaluations. Postponing to Section 4 the discussion of the results for similar distribution functions,

an analytical idea of the implications of (31) can be obtained in the limit $\psi(v|\rho) = \delta(v - V(\rho))$, which means that all cells move with a density dependent speed $V(\rho)$. In this case, denoting by

$$f(v) = \frac{\hat{\gamma}_c(k)\left(\sigma + \frac{1}{\mathcal{V}}\right) + \hat{\gamma}_s(k)kv}{\left(\sigma + \frac{1}{\mathcal{V}}\right)^2 + k^2v^2},$$

we have that

$$\int_0^U f(v)\frac{\partial \psi}{\partial \rho}(v|1)dv = \left[\frac{\partial}{\partial \rho}\int_0^U f(v)\psi(v|\rho)dv\right]\Big|_{\rho=1} = \frac{\partial}{\partial \rho}f(V(\rho))\Big|_{\rho=1} = \left[\frac{d}{dv}f(V(\rho))V'(\rho)\right]\Big|_{\rho=1}.$$

The limit of a delta distribution function then allows to compute the integral in (31) to get

$$1 = \frac{1}{\mathcal{V}}\left[\frac{\sigma + \frac{1}{\mathcal{V}}}{\left(\sigma + \frac{1}{\mathcal{V}}\right)^2 + k^2}\right] - \frac{M}{\mathcal{V}}\frac{\left[\left(\sigma + \frac{1}{\mathcal{V}}\right)^2 - k^2\right]k\hat{\gamma}_s(k) - 2\left(\sigma + \frac{1}{\mathcal{V}}\right)k^2\hat{\gamma}_c(k)}{\left[\left(\sigma + \frac{1}{\mathcal{V}}\right)^2 + k^2\right]^2}, \tag{32}$$

leading to the dispersion relation

$$\begin{aligned}\sigma^4 + \frac{3}{\mathcal{V}}\sigma^3 + \sigma^2\left(2k^2 + \frac{3}{\mathcal{V}^2} + \frac{kM\hat{\gamma}_s(k)}{\mathcal{V}}\right) + \sigma\left(\frac{1}{\mathcal{V}^3} + \frac{3k^2}{\mathcal{V}} - \frac{2k^2M\hat{\gamma}_c(k)}{\mathcal{V}} + \frac{2kM\hat{\gamma}_s(k)}{\mathcal{V}^2}\right)\\ +k^4 + \frac{k^2}{\mathcal{V}^2} - \frac{2k^2M\hat{\gamma}_c(k)}{\mathcal{V}^2} + \frac{kM\hat{\gamma}_s(k)}{\mathcal{V}^3} - \frac{k^3M\hat{\gamma}_s(k)}{\mathcal{V}} = 0\,.\end{aligned} \tag{33}$$

The application of the Hurwitz criterion allows to state that the equilibrium state is stable if

$$A := \left(1 + \frac{2}{3}M\hat{\gamma}_c(k)\right)k^2 + \frac{1}{3}\frac{M}{\mathcal{V}}k\hat{\gamma}_s(k) + \frac{8}{3\mathcal{V}^2}\,, \tag{34}$$

$$\begin{aligned}B := \frac{1}{A}\Bigg[&-\frac{4}{3}\frac{M^2}{\mathcal{V}}k^4\hat{\gamma}_c^2(k) + 2\left(3 + \frac{1}{3}M\hat{\gamma}_c(k)\right)\frac{M}{\mathcal{V}^2}k^3\hat{\gamma}_s(k)\\ &+2\left(3 + \frac{2}{3}M\hat{\gamma}_c(k) + \frac{1}{3}M^2\hat{\gamma}_s^2(k)\right)\frac{k^2}{\mathcal{V}^3} + \frac{8}{3}\frac{M}{\mathcal{V}^4}k\hat{\gamma}_s(k) + \frac{8}{3\mathcal{V}^5}\Bigg],\end{aligned} \tag{35}$$

$$C := k^4 - k^3\frac{M}{\mathcal{V}}\hat{\gamma}_s(k) + (1 - 2M\hat{\gamma}_c(k))\frac{k^2}{\mathcal{V}^2} + k\frac{M}{\mathcal{V}^3}\hat{\gamma}_s(k)\,, \tag{36}$$

are all positive. In the following we will try to establish the ranges of parameters $(M, \mathcal{V})$ leading to stability or instability. In particular, we will analyze if there exist wave numbers k such that at least one eigenvalue σ that is a root of (33) is positive. We recall that, as the wavelength is defined as $\frac{2\pi}{k}$, small values of k correspond to long waves and large values of k to short waves.

3.2 Short and long wave analysis

We will first focus on the case in which cells only evaluate the cell density on their membrane at a given distance from their center. This corresponds to a Dirac delta sensing kernel $\gamma(\lambda) = \delta(\lambda - 1)$ where 1 corresponds to the dimensionless sensing radius. For this localized sensing kernel, one trivially has that $\hat{\gamma}_s(k) = \sin(k)$ and $\hat{\gamma}_c(k) = \cos(k)$. Therefore, in the limit of very short waves we

have that A in (34) might become negative if $M > \frac{3}{2}$. Furthermore, the leading term in (35) is the first term in the square parenthesis which, independently of M and $\mathcal{V}$, is negative $\forall k \neq \frac{\pi}{2} + j\pi$, $j \in \mathbb{N}$. This implies that for values of k that are large enough, the product AB is always negative, so that A and B can not have the same sign. This implies that there is always a short wave instability for any value of M and $\mathcal{V}$. In conclusion, one has that the following statement holds:

Proposition 3.1. *Let us consider Eq.* (21) *with* $d = 1$ *and* $\psi(v|\rho) = \delta(v - V(\rho))$. *Then the uniform equilibrium distribution* (22) *is always unstable to short waves if the sensing kernel* γ *is a Dirac delta.*

If, instead, the kernel has a compact support in $[0, 1]$ and is differentiable therein, then the following statement holds

Proposition 3.2. *Let us consider Eq.* (21) *with* $d = 1$ *and* $\psi(v|\rho) = \delta(v - V(\rho))$, *and a sensing kernel* γ *having compact support in* $[0, 1]$ *and differentiable therein. Therefore*
– If γ *vanishes in 1, then the uniform equilibrium distribution* (22) *is always stable to short waves.*
– If γ *has a jump discontinuity in 1, then the uniform equilibrium distribution is unstable to short waves if*

$$M\mathcal{V} > \frac{9}{4}\frac{\gamma_0}{\gamma_1}\Gamma\left[1 + \sqrt{1 - \frac{\gamma_1^2}{9\gamma_0^2}}\right], \tag{37}$$

where $\gamma_0 = \gamma(0)$ *and* $\gamma_1 = \lim_{\lambda\to 1^-}\gamma(\lambda)$.

In fact, integrating by parts $\hat{\gamma}_c(k)$ and $\hat{\gamma}_s(k)$ one can readily have that for large values of k they behave like, to the leading order,

$$\hat{\gamma}_c(k) \approx \frac{\gamma_1 \sin(k)}{\Gamma k}, \quad \text{and} \quad \hat{\gamma}_s(k) \approx \frac{\gamma_0 - \gamma_1\cos(k)}{\Gamma k}.$$

Then, considering the leading order terms one has that $A \approx k^2$, $C \approx k^4$ and

$$B \approx \frac{6}{\mathcal{V}^3}k^2 g(k) \quad \text{where} \quad g(k) = 1 + 1\frac{\gamma_0 - \gamma_1\cos(k)}{\Gamma}M\mathcal{V} - \frac{2}{9}\left(\frac{\gamma_1\sin(k)}{\Gamma}\right)^2 M^2\mathcal{V}^2. \tag{38}$$

The sign of B depends on the sign of $g(k)$ whose derivative is

$$g'(k) = \frac{\gamma_1}{\Gamma}\sin(k)\left(1 - \frac{4}{9}\frac{\gamma_1}{\Gamma}\cos(k)\, M\mathcal{V}\right)M\mathcal{V}.$$

If $\gamma_1 = 0$, yielding a continuous sensing kernel in $\mathbb{R}$, then from (38) one readily has that $g(k)$, and B as a consequence, are always positive. Hence, one can never have instability to short waves.

If, instead, $\gamma_1 \neq 0$, yielding a discontinuous sensing kernel in $\mathbb{R}$, then the critical points of g are obtained for the values of k such that $\sin(k) = 0$ and if $M\mathcal{V} > \dfrac{9\Gamma}{4\gamma_1}$ for the values of k such that $\cos(k) = \dfrac{9\Gamma}{4\gamma_1 M\mathcal{V}}$. Now, for the former set of critical points the function g is always positive, *i.e.* $g(k : \sin(k) = 0) > 0$ and therefore the uniform configuration is stable to short waves. If $M\mathcal{V} > \dfrac{9\Gamma}{4\gamma_1}$, then substituting the latter set of critical points in (38) gives that $g(k)$ can become negative if

$$9 - 72\frac{\gamma_0}{\Gamma}M\mathcal{V} + 16\frac{\gamma_1^2}{\Gamma^2}M^2\mathcal{V}^2 > 0, \tag{39}$$

whose solution leads to the stated condition (37) for instability to short waves.

For instance, in the case of a uniform kernel $\gamma(\lambda) = H(1-\lambda)$, where H is the Heaviside function, we have that $\hat{\gamma}_s(k) = \frac{1-\cos(k)}{k}$ and $\hat{\gamma}_c(k) = \frac{\sin(k)}{k}$, and short waves are unstable when

$$M\mathcal{V} > \frac{9}{4} + 3\frac{\sqrt{2}}{2}\,. \tag{40}$$

In order to discuss the long wave limit, we start by observing that for $k = 0$ there are three negative eigenvalues equal to $-1/\mathcal{V}$ and one vanishing eigenvalue. An expansion of (33) or of (34)–(36) for long waves, *i.e.*, $k \approx 0$, leads to the instability criterion

$$(2M-1)\mathcal{V} - M\Gamma_1 > 0\,, \qquad \text{where} \quad \Gamma_1 = \frac{1}{\Gamma}\int_0^1 \lambda\gamma(\lambda)\,d\lambda\,.$$

Hence, we have instability to long waves if

$$M > \frac{1}{2} \quad \text{and} \quad \mathcal{V} > \frac{\Gamma_1 M}{2M-1}\,, \tag{41}$$

where, for instance, $\Gamma_1 = 1$ for a Dirac delta sensing kernel, $\Gamma_1 = 1/2$ for a uniform sensing kernel, and $\Gamma_1 = 1/3$ for a ramp sensing kernel defined as

$$\gamma(\lambda) = D(\lambda) := a(1-\lambda)_+. \tag{42}$$

3.3 Evaluation of the dispersion relation

The analysis above allows to state that for a Dirac delta sensing kernel the uniform distribution p_∞ is always unstable at least to short waves. On the other hand, for more regular kernels there are regions in the M-$\mathcal{V}$ parameter space where the uniform distribution is stable to both long and short waves. In order to complete the stability analysis, having set a pair of values $(M, \mathcal{V})$, we solve the dispersion relation (33) for any k to find the four roots as a function of k. As already stated for $k = 0$ there are three roots equal to $-1/\mathcal{V}$, while the fourth one vanishes. So, this last root is most likely the one that for some wave numbers might have a positive real part $\mathcal{R}(\sigma)$ leading to instability, as we actually found in all our evaluations. We then define the wave number k_{max} as the maximum argument of $\mathcal{R}(\sigma)$ over k, *i.e.*,

$$k_{max} = argmax_{k\in\mathbb{R}_+}\mathcal{R}(\sigma)(k) \tag{43}$$

that is the wave number corresponding to the maximum of the real part of the eigenvalue σ.

We are now going to plot $\mathcal{R}(\sigma)$ for different sensing kernels in order to determine if there are unstable wave numbers. We know that if the sensing kernel is a Dirac delta this will certainly be the case because we have theoretically shown that short waves are always unstable. As an example, in Fig. 1a,d we plot the typical behaviour of the eigenvalue with maximum real part for a Dirac delta sensing kernel. Figure 1a corresponds to small values of M and $\mathcal{V}$ that do not satisfy (41). In fact, long waves are stable and in order to have instability we need to look at higher values of the wave number k, for example $k > 10$. Figure 1d corresponds to higher values of M and $\mathcal{V}$ that satisfy (41). This implies that there is instability also for small values of k, as put in evidence in Fig. 1g that is a zoomed in of Fig. 1d in the small k region. A common feature of the behaviour of the real part of the eigenvalue for all parameters M and $\mathcal{V}$ is the oscillation from a (negative) nearly constant value to an increasing maximum value. Hence, the most unstable waves are those with very small wavelength leading to a catastrophic instability with $k_{max} \to \infty$.

In this respect a remark is needed grounded on the fact that cells have a finite diameter d. This distance d determines when cells come in contact. An instability with wavelength smaller than d has little biological sense. From the quantitative point of view, if $d \approx 20\,\mu$m and cells can extend up to $R \approx 100\,\mu$m, then the above remark suggests to restrict the analysis to $k < 2\pi\frac{R}{d} \approx 10\pi$, though the model can in principle be applied to larger values of k.

Concerning more regular sensing kernels, the stability of the equilibrium configuration to short waves is possible as stated in Proposition 3.2. In particular, stability to short waves holds true

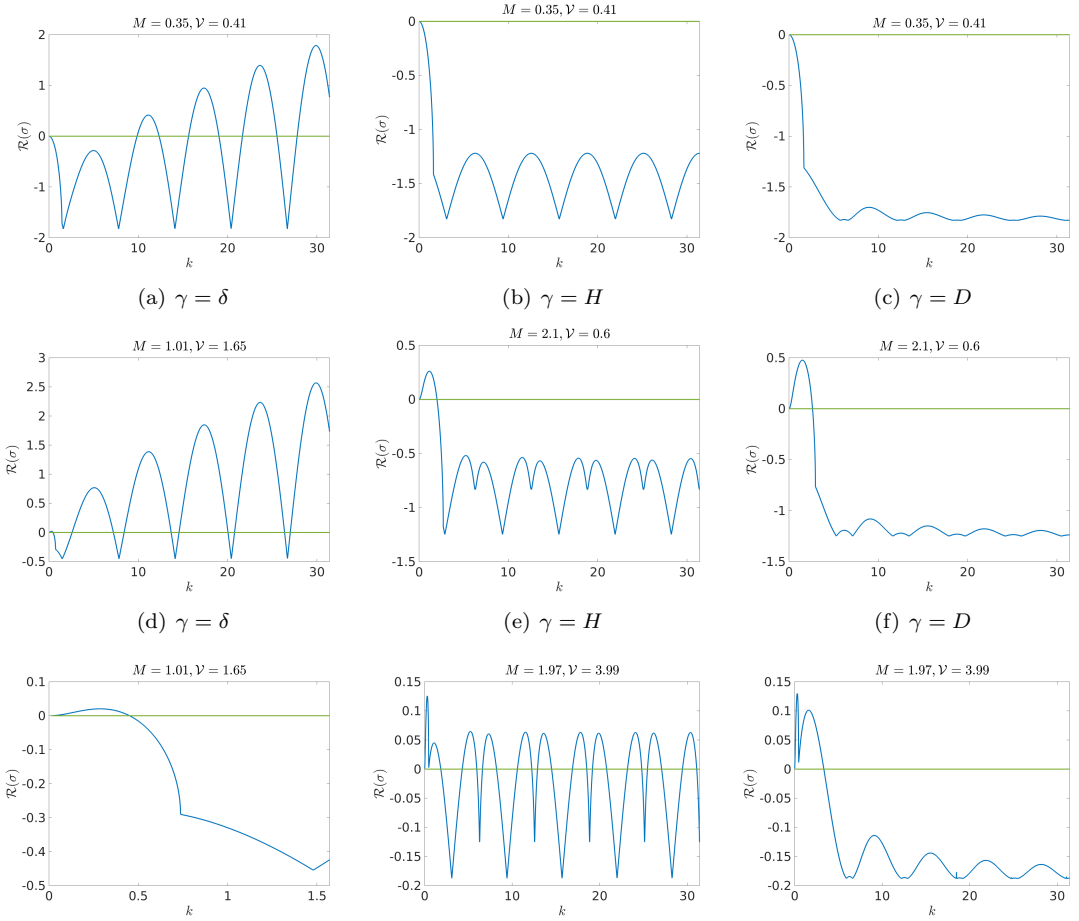

(a) $\gamma = \delta$ (b) $\gamma = H$ (c) $\gamma = D$

(d) $\gamma = \delta$ (e) $\gamma = H$ (f) $\gamma = D$

(g) $\gamma = \delta$ (h) $\gamma = H$ (i) $\gamma = D$

Figure 1: Real part of the eigenvalue σ that vanishes for $k = 0$ as a function of the wave number k for a Dirac delta sensing kernel (first column), Heaviside sensing kernel (second column), and ramp sensing kernel (42) (third column) for some sample values of M and $\mathcal{V}$. Specifically, the first and second row correspond to values for which long waves are stable and unstable, respectively, for both the uniform and the ramp sensing kernels. In the third row, (g) is a zoomed in view of (d) focusing on the long wave region. (h) and (i) refer to values of M and $\mathcal{V}$ corresponding to instability to short waves in the Heaviside sensing kernel case as put in evidence in (h), but not in the ramp sensing kernel case (i). However, in this case the uniform equilibrium configuration is still unstable to long waves.

for all values of $(M, \mathcal{V})$ if the sensing kernel is continuous (see the third column in Fig. 1), while it holds true only for small values of both M and $\mathcal{V}$ if the sensing kernel is discontinuous at the maximum value of the sensing radius, *i.e.*, $\lambda = R$ (see Figs. 1b,e) and might fail for larger values as shown in Fig. 1h.

Generally speaking, recalling (33), one readily has that its roots σ, and therefore their real part, are functions of $(k, M, \mathcal{V})$. In Fig. 2a,b we plot the surface in the $(k, M, \mathcal{V})$ space defined by $(k, M, \mathcal{V})\ s.t.\ \mathcal{R}(\sigma) = 0$. The region beyond the surface from the reader viewpoint corresponds to unstable wave numbers. In order to relate these plots with those in the second and third column of Fig. 1, respectively, it is useful to imagine to draw a line starting from $k = 0$ for a fixed value of the pair $(M, \mathcal{V})$. The intersections of the line with the green surface correspond to the values in Fig. 1 for which the curve crosses the x axis. Coherently with Proposition 3.2, for the ramp kernel (42) the surface lies in the region with low values of k, as it is continuous in $\lambda = R$ (see Fig.

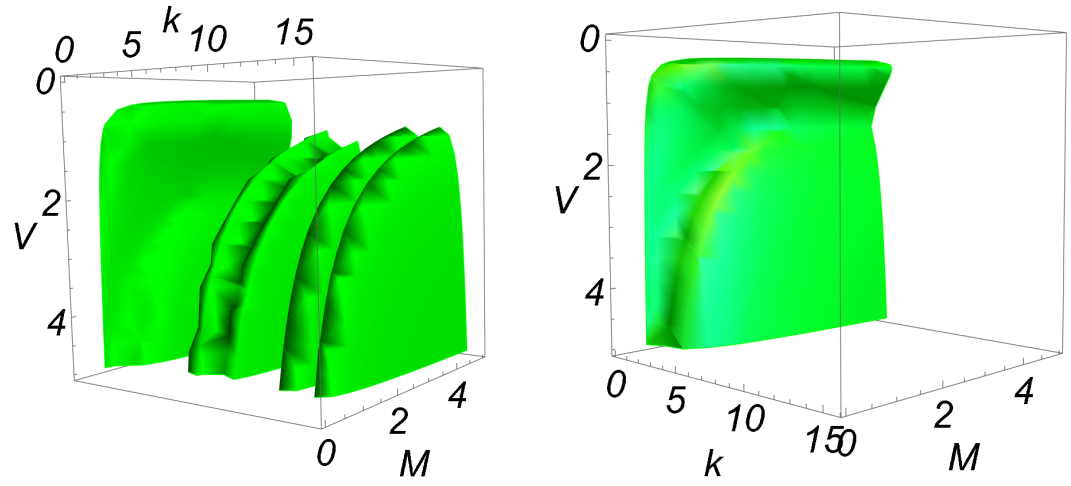

(a) $\gamma = H$ (b) $\gamma = D$

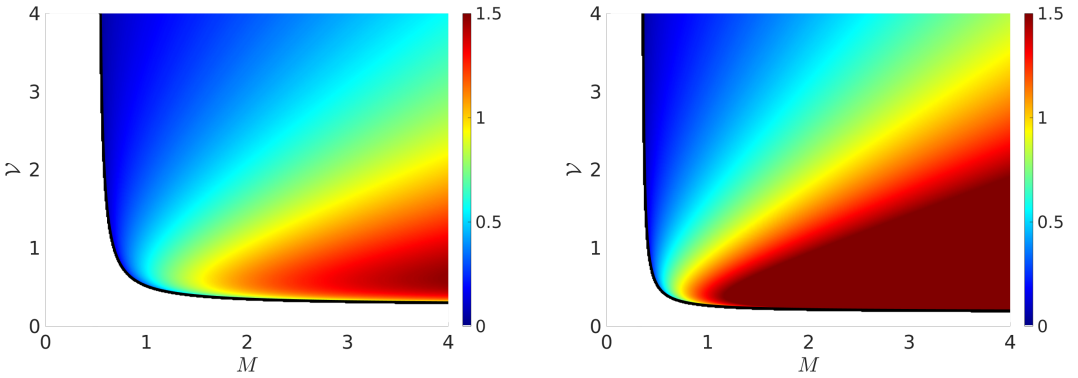

(c) $\gamma = H$ (d) $\gamma = D$

Figure 2: Top row: Surface in the three-dimensional subspace $(k, M, \mathcal{V}) \in [0, 10\pi] \times [0, 5] \times [0, 5]$ where the real part of a root of the dispersion relation vanishes, *i.e.*, $\mathcal{R}(\sigma) = 0$ (while the positive parts of the other three roots are negative). Bottom row: Plot of the function $k_{max} = argmax_{k\in[0,10\pi]}\mathcal{R}(\sigma)$ as a function of M and $\mathcal{V}$. The white regions correspond to pairs of parameters $(M, \mathcal{V})$ for which the homogeneous equilibrium configuration is stable. The black thick line corresponds to the curve predicted by the theoretical long wave instability criterion given in (41).

2b). Specifically, if $M = 0.35$ and $\mathcal{V} = 0.41$ the line starting from $k = 0$ runs close to the top left edge without intersecting the surface, as in Fig. 1c where the plot does not intersect the x-axis. Instead, if $M = 2.1$ and $\mathcal{V} = 0.6$, as in Fig. 1i, the line starts beyond the surface corresponding to long wave instability crossing it for $k \approx 3.3$ as it runs close to a middle line of the base of the cube in the figure. On the other hand, for a uniform kernel (see Fig. 2a) there are additional regions in which $\mathcal{R}(\sigma) > 0$. In fact this happens for high wave numbers and high values of M and $\mathcal{V}$, *i.e.*, if (40) is satisfied. For instance, these regions are not crossed when $M = 2.1$ and $\mathcal{V} = 0.6$ (corresponding to Fig. 1e) while they are crossed if $M = 1.97$ and $\mathcal{V} = 3.99$ corresponding to Fig. 1h.

Figure 2c,d reports the wave number k_{max} defined in (43) as a function of $(M, \mathcal{V})$. The white region corresponds to linear stability, *i.e.* $\mathcal{R}(\sigma) < 0 \ \ \forall k$. Its border perfectly matches with the predictions of the the stability criterion with respect to long waves (41) highlighted by the thick black line. The colored region in 2c,d also corresponds to the intersection of the green surface in Figure 2a,b, respectively with the hyperplane $k = 0$. We remark that the theoretical curve (41) perfectly catches the onset of instability, because below the thick black curve, not only waves with $k \to 0$ and $k \to \infty$ are stable, but also those with any wave number k. Referring to specific values of the parameters used in Fig. 1, for $(M, \mathcal{V}) = (2.1, 0.6)$, we have $k_{max} \approx 1$ for the uniform kernel and $k_{max} \approx 1.5$ for the ramp sensing kernel.

Concerning the uniform kernel, when (40) is satisfied by the pair of parameters $(M, \mathcal{V})$, there are several intervals of k where $\mathcal{R}(\sigma) > 0$ (see Fig. 2a). However, like in Fig. 1h, k_{max} is always in the first of these intervals. This is also evident in Fig. 2c that shows that for $M, \mathcal{V} < 4$, $k_{max} < 1.5$. This implies that instability occurs at a finite wavelength $2\pi/k_{max}$ that is longer than $4\pi/3$.

The same analysis can be done for a smooth ramp kernel in Fig. 2b,d. We recall that in this case Proposition 3.2 states that the equilibrium configuration is stable to perturbations corresponding to short waves. This is coherent with the fact that in Fig. 2b we have that $\mathcal{R}(\sigma) > 0$ only for small values of k and when the condition (41) is satisfied (represented again by the intersection of the green surface with the hyperplane $k = 0$). Looking at Fig. 2d again, we observe that for the range of parameters reported, the black thick curve corresponding to the stability criterion with respect to long waves (41) well divides the stability region from the one where we have instability to waves characterized by a wavelength higher than $4\pi/3$.

4 Numerical tests

In this section we want to compare the predictions deriving from the linear stability analysis with the results of the simulation of the original kinetic model (11). We remark that the results of the linear stability analysis are obtained in the limit case given by $\psi(v|\rho) = \delta(v - \bar{v}(\rho))$ that allowed to simplify (31) into (32). Instead, the simulation of the kinetic model will be obtained with a smooth probability density distribution, namely a von Mises distribution

$$\psi(v|\rho) = A \exp\left(\cos\left(\frac{B\pi}{U}(v - \bar{v}(\rho))\right)\right), \tag{44}$$

where A is a normalization constant and B is such that the variance of ψ is 0.02 and with a mean given by (13). If $B \to \infty$ the von Mises distribution converges to a Dirac delta. We numerically integrate Eq. (11) with specular reflective boundary conditions that are no-flux boundary conditions at the macroscopic level [16, 21].

The numerical method adopted consists in a first order splitting for the relaxation and transport step that we perform using a Van Leer scheme. For further details, we refer the reader to [10] and [16, 17].

In Fig. 3 we report the results obtained using a Dirac delta sensing kernel and still a von Mises distribution for ψ. In the previous section we have showed analytically that in the limit case in which we set ψ equal to a Dirac delta, then any uniform configuration is catastrophically unstable to very short waves ($k \gg 1$). Of course, we can not strictly apply the statement of Proposition 3.1 in the case of a von Mises distribution, but could expect that for very small variances the

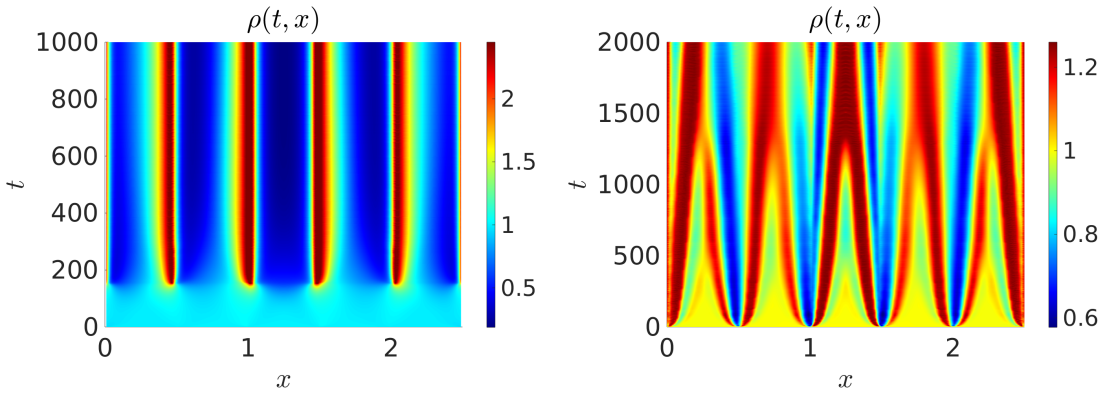

(a) $M = 4.13$, $\mathcal{V} = 0.015$

(b) $M = 4.13$, $\mathcal{V} = 0.005$

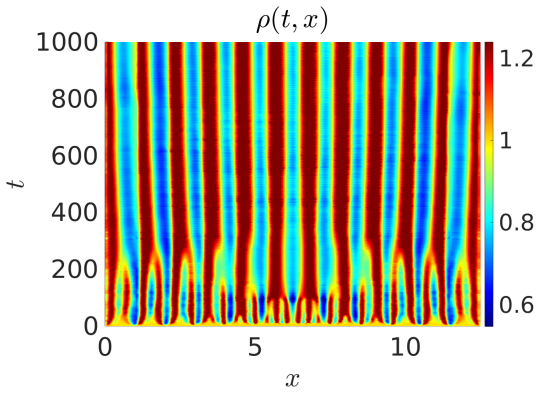

(c) $M = 0.68$, $\mathcal{V} = 0.02$

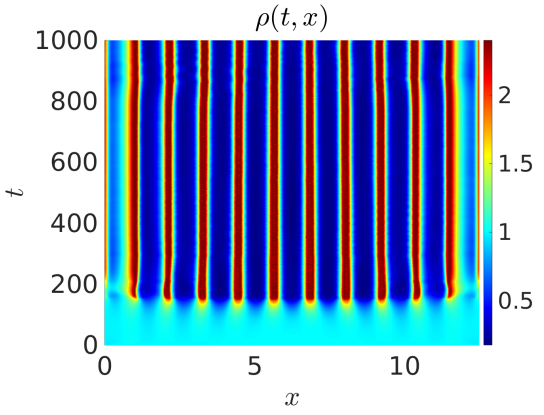

(d) $M = 0.68$, $\mathcal{V} = 0.008$

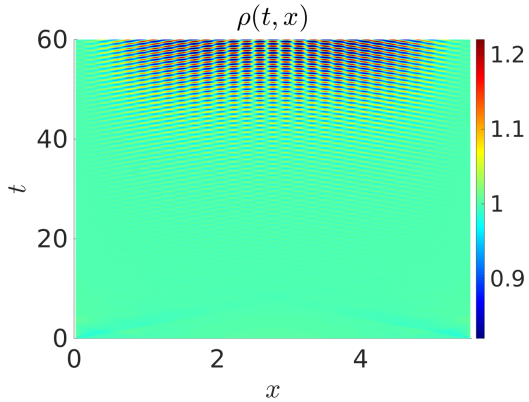

(e) $M = 0.35$, $\mathcal{V} = 0.41$

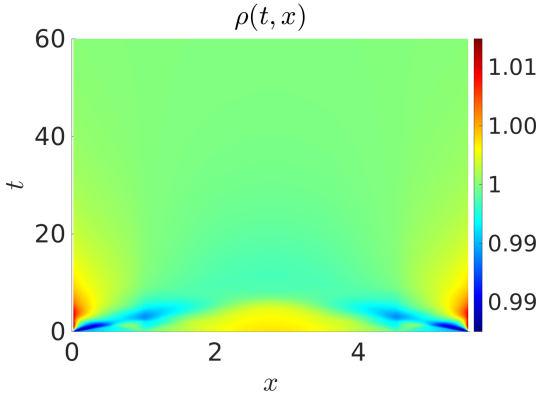

(f) $M = 0.35$, $\mathcal{V} = 0.41$

Figure 3: Time evolution of the macroscopic cell density $\rho(t,x)$: pattern formation for a Dirac delta sensing kernel. In all cases the variance of the von Mises distribution is 0.02 but for (f) where the variance is 0.09. The values of the dimensionless parameter ρ_{th} are: (a) 2.48, (b) 1.24, (c) 1.24, (d) 2.48, (e)-(f) 3.38.

behaviour is close to that theoretically predicted. Of course, in principle there is a limit value to the shortest wavelength testable related to the mesh size used in the simulation. However, our simulations do not suffer from this criticality. In fact, it is observed that using a von Mises distribution for ψ results in the formation of patterns with wavelength much larger than the mesh size, that in our case was $dx = 0.01$. To illustrate this, in Fig. 3 we show patterns for values of the variance corresponding to 0.02 characterized by a size at least one order of magnitude larger. Actually, the fact that the variance has a stabilizing effect is put in evidence by a comparison of Fig. 3e and f obtained using variances equal to 0.02 and 0.09, respectively.

Turning to more regular kernels, we have observed that also in the nonlinear regime and for a smooth probability density distribution ψ no instability occurs for values of $(M, \mathcal{V})$ for which the uniform configuration is linearly stable (not shown). Figure 4, instead, shows some patterns obtained for higher values of $(M, \mathcal{V})$ for which linear instability occurs for long waves. In particular, in the caption we report the values of k_{max} and the relative wavelength $\Lambda = 2\pi/k_{max}$ that can be read from Fig. 2a (obtained from the linear stability analysis) for the values of $(M, \mathcal{V})$ used. In 4a,b the pattern wavelength that we can observe in the developing pattern well corresponds to the Λ predicted by the linear stability analysis. In 4c,d it seems that initially a wavelength that is close to the most unstable one is triggered, but later on the two central peaks merge into one bigger plateau. We remark that in all cases the dimensionless density never overcomes the values corresponding to ρ_{th} and therefore to the physical limit of migration.

We finally observe that using the same values of the parameters and a ramp kernel we obtain very close results in 4a,b (not shown) and only a slight difference between 4c and d. In fact, the values of k_{max} for the ramp sensing kernel corresponding to the values of $(M, \mathcal{V})$ in Fig. 4a and b are 0.37 (see Fig. 2a) and 0.3 (see 2b) respectively, that determine values of Λ that are very close to the ones that we can observe in Fig. 4a,b. We cannot make the same comparisons concerning the wavelength in Fig. 3, *i.e.*, for the Dirac delta sensing kernel, as in this case we have instability to very short waves.

5 Discussion

We performed a linear stability analysis of a kinetic equation with a non-linear velocity jump operator, in which the kernel depends on the macroscopic density. We find that in the general d-dimensional case the eigenvalue is determined by an integral condition involving the wavelength and two dimensionless parameters. The first one $\mathcal{V}$, defined in (18), involves the turning frequency, the sensing radius and the speed. As such, it describes the stiffness of the system, playing the role of a sort of Knudsen number. The second one measures the variation of the speed probability density distribution with respect to the cell density at the homogeneous configuration. In the case of a Dirac delta it reduces to the derivative of the density dependent mean speed computed at the homogeneous configuration and is represented by the dimensionless parameter M. The two parameters are inter-dependent as they both depend on the uniform configuration ρ_∞ and on the threshold value ρ_{th}, but they can not be combined in a unique parameter as in [18]. Both in the linear stability analysis done here and in [18], the stiffness parameter $\mathcal{V}$ discriminates between stable and unstable configurations, even for fixed values of the uniform density ρ_∞. However, in the present case, also the parameter M plays a similar role.

The deep intimate difference between the two models lies in the fact that in [18] the cell density influences the polarization of cells but not their speed. It is then used to describe both adhesion and contact inhibition of locomotion phenomena (see [7] and references therein) keeping the same speed probability density distribution. This implies that the parameter $\mathcal{V}$ does not depend on the macroscopic cell density and is the reason why the two non-dimensional parameters may be unified in a unique parameter determining linear stability or instability.

In contrast, in the present work cells polarize randomly and their speed decreases with the macroscopic cell density. In particular, it vanishes as the macroscopic cell density reaches a threshold value ρ_{th}, corresponding to a jammed situation in which cells can not move. Therefore, the ratio between the the uniform density ρ_∞ and ρ_{th} determine both M and $\mathcal{V}$. This is the

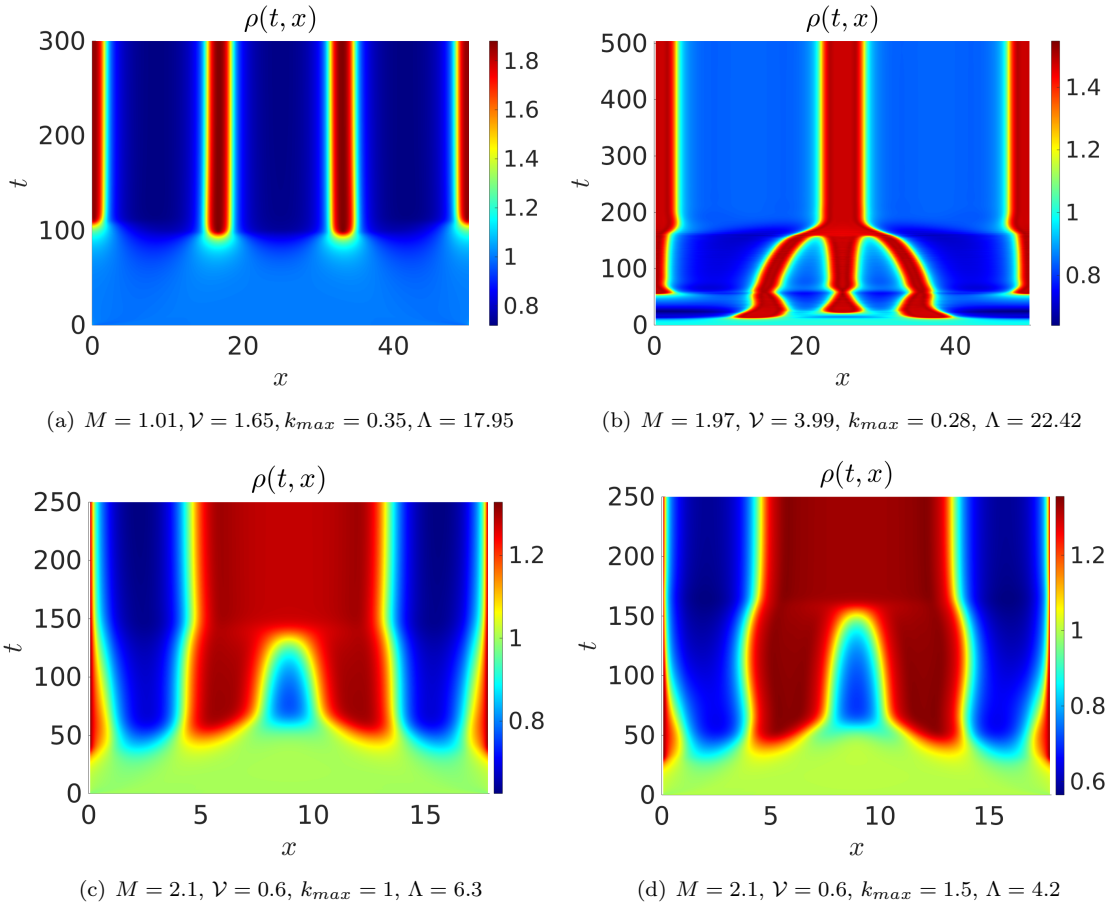

(a) $M = 1.01, \mathcal{V} = 1.65, k_{max} = 0.35, \Lambda = 17.95$

(b) $M = 1.97$, $\mathcal{V} = 3.99$, $k_{max} = 0.28$, $\Lambda = 22.42$

(c) $M = 2.1$, $\mathcal{V} = 0.6$, $k_{max} = 1$, $\Lambda = 6.3$

(d) $M = 2.1$, $\mathcal{V} = 0.6$, $k_{max} = 1.5$, $\Lambda = 4.2$

Figure 4: Time evolution of the macroscopic cell density: pattern formation for uniform and ramp kernels. In (a) and (b) only the results for the uniform kernel are reported because those obtained with a ramp kernel are very similar. A slight difference can be seen for $M = 2.1$ and $\mathcal{V} = 0.6$ between the pattern obtained using the uniform kernel in (c) and the ramp kernel in (d). The linear stability values of k_{max} and most unstable wavelength are also reported for visual comparison. The values of the dimensionless parameter ρ_{th} are: (a) 1.24, (b) 1.5 and (c)-(d) 1.48.

reason why in the present work there are two separate dimensionless parameters, the linear stability criterion can not be expressed in terms of a unique parameter, and the dispersion relation obtained in the one-dimensional case is a fourth degree polynomial.

We performed a long and short wave analysis and evaluated numerically the solution of the dispersion relation for all wave numbers. The analysis shows that the stability of the homogeneous equilibrium is deeply related to the sensing kernel γ. If it is a Dirac delta, *i.e.*, the cell samples the cell density only at a fixed sensing radius, then the uniform configuration is always unstable to short waves with oscillating eigenvalues with peaks that increase with the wave number. Conversely, for more regular sensing kernels like the ramp kernel that weights the density in a linear decreasing way starting from the cell nucleus, then the uniform configuration is always stable to short waves. On the other hand, for uniform sensing kernels there is short wave instability under given conditions identified by (40). In the last two cases there is an instability region for high values of M and $\mathcal{V}$ above the hyperbolas defined by (41) with asymptotes $M = 1/2$ and $\mathcal{V}$ equal to $1/2$ in the case of a uniform kernel and $1/3$ in the case of a ramp kernel.

The simulations performed with a von Mises probability density distribution for the velocity speed fit well with the theoretical results in the case of the uniform and of the ramp kernels, while

in the case of Dirac delta sensing kernel instability to larger, yet finite, wave numbers is shown.

We remark that in this paper we focused on volume filling effects influencing cell speed but not orientation. A natural development of the model would then be to extend the analysis done here and in [18] including both phenomena in the model. This is important, in order to include cell-cell adhesion phenomena, which are neglected here, but can have an impact both on cell polarization and speed. In fact, the coupling of cell-cell adhesion and volume filling is a fundamental feature in collective cell migration, that is at the basis of tissue formation and cancer spread.

Acknowledgements

This work was partially supported by Istituto Nazionale di Alta Matematica, Ministry of Education, Universities and Research, through the MIUR grant Dipartimenti di Eccellenza 2018-2022, Project no. E11G18000350001, and the Scientific Reseach Programmes of Relevant National Interest project n. 2017KL4EF3. N.L. acknowledges Compagnia di San Paolo (Torino, Italy).

References

[1] N. J. Armstrong, K. J. Painter, and J. A. Sherratt. A continuum approach to modelling cell-cell adhesion. *Journal of Theoretical Biology*, 243(1):98–113, 2006.

[2] S. Blandin and P. Goatin. Well-posedness of a conservation law with non-local flux arising in traffic flow modeling. *Numerische Mathematik*, 132, 2015.

[3] C. Cercignani. *The Boltzmann Equation and its Applications*. Springer, New York, 1987.

[4] A. Chauviere, T. Hillen, and L. Preziosi. Modeling cell movement in anisotropic and heterogeneous network tissues. *Networks & Heterogeneous Media*, 2(2):333–357, 2007.

[5] A. Chauviere, T. Hillen, and L. Preziosi. Modeling the motion of a cell population in the extracellular matrix. *Discrete and Continuous Dynamical Systems B*, 2007(Supplemental volume):250–259, 2007.

[6] F. A. Chiarello. An overview of non-local traffic flow models. 2019.

[7] A. Colombi, M. Scianna, K. Painter, and L. Preziosi. Modelling chase and run migration in heterogeneous populations. *Journal of Mathematical Biology*, 80:423–456, 2020.

[8] R. Eftimie, G. de Vries, M. A Lewis, and F. Lutscher. Modeling group formation and activity patterns in self-organizing collectives of individuals. *Bulletin of Mathematical Biology*, 69:1537–65, 2007.

[9] R. Eftimie, G. Vries, and M. Lewis. Complex spatial group patterns result from different animal communication mechanisms. *Proceedings of the National Academy of Sciences of the United States of America*, 104:6974–9, 2007.

[10] F. Filbet and K. Yang. Numerical simulation of kinetic models for chemotaxis. *SIAM Journal on Scientific Computing, Society for Industrial and Applied Mathematics*, 36(3):B348–B366, 2014.

[11] M. Herty, G. Puppo, S. Roncoroni, and G. Visconti. The BGK approximation of kinetic models for traffic. *Kinetic and Related Models*, 13:279, 2020.

[12] T. Hillen. M5 mesoscopic and macroscopic models for mesenchymal motion. *Journal of Mathematical Biology*, 53:585–616, 2006.

[13] T. Hillen, K. J. Painter, and C. Schmeiser. Global existence for chemotaxis with finite sampling radius. *Discrete & Continuous Dynamical Systems - B*, 7(1):125–144, 2007.

[14] B. S. Kerner. *The Physics of Traffic. Understanding Complex Systems*. Springer, Berlin, 2004.

[15] M. Krasnianski, K. Painter, C. Surulescu, and A Zhigun. Nonlocal and local models for taxis in cell migration: a rigorous limit procedure. Preprint: `arixiv` 1908.10287.

[16] N. Loy and L. Preziosi. Kinetic models with non-local sensing determining cell polarization and speed according to independent cues. *Journal of Mathematical Biology*, 80:373–421, 2019.

[17] N. Loy and L. Preziosi. Modelling physical limits of migration by a kinetic model with non-local sensing. *Journal of Mathematical Biology*, 80:175–1801, 2020.

[18] N. Loy and L. Preziosi. Stability of a non-local kinetic model for cell migration with density dependent orientation bias. *Kinetic and related models*, 13(5):1007–1027, 2020.

[19] H. G. Othmer, S. R. Dunbar, and W. Alt. Models of dispersal in biological systems. *Journal of Mathematical Biology*, 26(3):263–298, 1988.

[20] H. G. Othmer and T. Hillen. The diffusion limit of transport equations II: Chemotaxis equations. *SIAM Journal of Applied Mathematics*, 62:1222–1250, 2002.

[21] R. G. Plaza. Derivation of a bacterial nutrient-taxis system with doubly degenerate cross-diffusion as the parabolic limit of a velocity-jump process. *Journal of Mathematical Biology*, 78:1681–1711, 2019.

[22] G. Puppo, M. Semplice, A. Tosin, and G. Visconti. Fundamental diagrams in traffic flow: The case of heterogeneous kinetic models. *Communications in mathematical sciences*, 14:643–669, 2016.

[23] G. Puppo, M. Semplice, A. Tosin, and G. Visconti. Kinetic models for traffic flow resulting in a reduced space of microscopic velocities. *Kinetic and Related Models*, 10:823–854, 2017.

[24] D. W. Stroock. Some stochastic processes which arise from a model of the motion of a bacterium. *Zeitschrift für Wahrscheinlichkeitstheorie und Verwandte Gebiete*, 28(4):305–315, 1974.